enkephalin, eluted at 165 min, was collected and accounted for 92% of the starting material.

**(B) Bovine Growth Hormone Fragment (128–131).** The tetrapeptide Boc-Glu(OBzl)-Asp(OBzl)-Gly-Thr(Bzl)-$OCH_2$-resin was synthesized from Boc-Thr(Bzl)-$OCH_2$-resin (5 g, 0.22 mmol/g). Samples of 100–250 mg each were treated with different HF procedures as required. The results (Table VIII) were quantitated by ion-exchange chromatography on an AA-15 column (Beckman, 0.9 × 54 cm) attached on a Beckman 120B amino acid analyzer, eluted with pH 3.20 citrate buffer at 59 °C. The elution times of the peptides were $\beta$-peptide 53 min, $\alpha$-peptide 70 min, and imide 135 min (Scheme VI).

**(C) Pentagastrin Amide.** The pentapeptide Boc-Gly-Trp(For)-Met-(O)-Asp(OBzl)-Phe-NH-$CH(C_6H_5)$-$C_6H_4$-$OCOCH_2$-resin (**3**), was synthesized from a multidetachable benzhydrylamine-resin, prepared according to ref 46, 5 g, 0.18 mmol/g. Samples of 100–250 mg each were treated with different HF procedures as required. The results are summarized in Tables XII and XIII.

**Acknowledgment.** We thank D. Rosberger for technical assistance and M. LeDoux for the amino acid analysis. This work was supported in part by Grant AM 01260 from the U.S. Public Health Service.

**Registry No.** Boc-L-Ser(Bzl), 23680-31-1; Tyr(Bzl), 16652-64-5; Boc-Tyr(Bzl), 2130-96-3; L-Trp(For)·HCl, 38023-86-8; H-Gly-Trp-Met-Asp-Phe-$NH_2$, 18917-24-3; Boc-L-Trp(For), 47355-10-2; Z-Gly, 1138-80-3; Sor(Bzl), 4726-96-9; Thr(Bzl), 4378-10-3; Asp(OBzl), 2177-63-1; Glu(OBzl), 1676-73-9; His(Tos), 23241-48-7; Lys(2-ClZ), 42390-97-6; Boc-Ala, 15761-38-3; Z-Ala, 1142-20-7; Trp(For), 74257-18-4; Tyr(Bzl), 16652-64-5; Tyr(2,6-$Cl_2$Bzl), 40298-69-9; Tyr(BrZ), 86902-29-6; H-Gly-Trp-Met(O)-Asp-Phe-$NH_2$, 86941-81-3; H-Gly-Trp(For)-Met(O)-Asp-Phe-$NH_2$, 86921-21-3; H-Gly-Trp(For)-Met-(O)-Asp-Phe-$NH_2$, 86902-30-9; H-Gly-Trp(For)-Met-Asp-Phe-$NH_2$, 86941-82-4; hydrofluoric acid, 7664-39-3; dimethyl sulfide, 75-18-3; L-methionine sulfoxide, 3226-65-1; tri-*p*-tolyl trithioorthoformate, 17241-10-0; methionine enkephalin, 58569-55-4; bovine growth hormone fragment (125–131), 57680-10-1; anisole, 100-66-3; thioanisole, 100-68-5; diphenyl sulfide, 139-66-2; thiacyclopentane, 110-01-0; 1,4-thioxane, 15980-15-1; *p*-thiocresol, 106-45-6; ethanethiol, 75-08-1; ethanedithiol, 540-63-6; 3,4-dimercaptotoluene, 496-74-2; thiophenol, 108-98-5.

# Resonance Raman Spectra of Rubredoxin, Desulforedoxin, and the Synthetic Analogue $Fe(S_2$-*o*-$xyl)_2^-$: Conformational Effects

**Vittal K. Yachandra,[†] Jeffrey Hare,[†] I. Moura,[‡] and Thomas G. Spiro*[†]**

*Contribution from the Department of Chemistry, Princeton University, Princeton, New Jersey 08544, the Portugal and Gray Freshwater Biological Institute, Centro de Quimica Estrutural, I.S.T., 1000 Lisbon, Portugal, and the University of Minnesota, Minneapolis, Minnesota 55392.* *Received September 7, 1982*

**Abstract:** The resonance Raman (RR) spectrum of the rubredoxin analogue $Fe(S_2$-*o*-$xyl)_2^-$ ($S_2$-*o*-xyl = *o*-xylylene-$\alpha,\alpha'$-dithiolate) shows four widely spaced bands (I–IV) in the Fe–S stretching region, 297, 321, 350, and 374 $cm^{-1}$, instead of the two expected for tetrahedral $FeS_4$. The RR spectrum of oxidized rubredoxin ($Rd_{ox}$) is also shown to have four bands in this region, 312, 325, 359, and 371 $cm^{-1}$, contrary to an initial impression of a tetrahedral spectrum. Normal mode calculations were carried out to explore the possible sources of Fe–S mode splitting. For a $FeS_4$ model, distortions of the angles split the $T_2$ mode but only by small amounts for the angles seen in either the protein or the analogue crystal structures; the effect on the $A_1$ breathing mode was negligible. When coupling between Fe–S stretching and S–C–C bending was included, with $Fe(SCH_2CH_3)_4$ as a model (with point mass methyl and methylene groups), an appreciable effect of the S–C dihedral angles on the Fe–S breathing mode was observed, which accounted satisfactorily for the band I frequency difference between $Rd_{ox}$ and $Fe(S_2$-*o*-$xyl)_2^-$ on the basis of the differing S–C dihedral angles (90°, 180° and 90°, 90°, respectively, for the $C_2$-related pairs). This coupling also split the $T_2$ Fe–S components but not by enough to account for the observed spectra. Additional couplings were revealed by perdeuteration of the methylene groups in $Fe(S_2$-*o*-$xyl)_2^-$, which produced 10-$cm^{-1}$ *up*shifts of the middle two Fe–S bands (II and III). These upshifts could be explained by the crossing over of nearby ligand skeletal modes, observed in the IR spectrum, which shifted down strongly on methylene perdeuteration. Differential coupling with these ligand modes might account for the Fe–S mode splitting. $Rd_{ox}$ RR spectra from *Desulfovibrio gigas*, *Desulfovibrio sulfuricans*, and *Megasphera elsdenii* were very similar. The constancy of band I (312 $cm^{-1}$) implies the same set of S–C dihedral angles. Slight shifts in bands II and III were observed, suggesting subtle conformational differences. The RR spectrum of *D. gigas* desulforedoxin resembled that of rubredoxin but showed an appreciable upshift of band II, to 341 $cm^{-1}$, possibly reflecting S–Fe–S angle distortions that might be associated with the adjacency of two cysteine side chains in the primary structure.

The iron–sulfur proteins continue to attract much interest from inorganic and biochemists.[1] These ubiquitous electron-transfer proteins encompass several structural classes, with Fe–S centers containing one, two, three, or four iron atoms. They all absorb light strongly in the visible region, reflecting S → Fe charge-transfer electronic transitions. They are therefore good candidates for structural monitoring via resonance Raman (RR) spectroscopy,[2,3] since the Fe–S vibrational modes are expected to be selectively enhanced. Indeed, one of the first biological applications of RR spectroscopy was the study of rubredoxin, a one-Fe protein, by Long and co-workers.[4] In the intervening decade, however,

[†] Princeton University.
[‡] Portugal and Gray Freshwater Biological Institute and University of Minnesota.

(1) Spiro, T. G., Ed. "Iron-sulfur Proteins"; Wiley-Interscience: New York, 1982.
(2) Carey, P. R.; Solares, V. R. In "Advances in Infrared and Raman Spectroscopy"; Clark, R. J. H.; Hester, R. E., Ed.; Heyden: London, 1980; Vol. 7, Chapter 1.
(3) Spiro, T. G.; Gaber, B. P. *Annu. Rev. Biochem.* **1977**, *46*, 353.

0002-7863/83/1505-6455$01.50/0 

only fragmentary reports of Fe–S RR spectra have appeared.[5-11]

The slow development of Fe–S RR spectroscopy is attributable largely to experimental difficulties. Fe–S complexes are labile and are prone to decompose under laser irradiation. Moreover, the RR enhancements are lower than for other chromophores, such as hemes or polyenes, despite quite large molar absorptivities for the visible bands. The relatively low scattering power no doubt results from damping effects[14] associated with the great breadth of the absorption bands or, equivalently, from interferences among the many closely spaced charge-transfer transitions that contribute to the absorptions. Finally, Fe–S protein samples frequently show unacceptably high fluorescence backgrounds, which may arise from decomposition products or from flavin contaminants.

These difficulties have slowly yielded to improved techniques, and we have recently been able to obtain spectra of sufficient quality to begin characterizing the vibrational modes of the various Fe–S species. Our preliminary results have been summarized,[12] and reports have appeared on three-Fe and four-Fe proteins.[10,11] In the present study we return to the subject of one-Fe centers, whose RR spectra are shown to be considerably more complex than originally thought.[4] Subsequent papers characterize the vibrational modes of two-Fe[13] and four-Fe[14] centers.

## Materials and Methods

**Proteins.** Rubredoxin and desulforedoxin from *Desulfovibrio gigas* were isolated as described elsewhere.[16] Rubredoxin was prepared from *Desulfovibrio sulfuricans* (strain 27774) and from *Megasphera elsdenii*, by the methods described in ref 17 and 18, respectively. The 495/280 nm absorbance ratios were ~0.4. The proteins were further purified by Sephadex *G-100* filtration and DEAE-52 ion-exchange fractionation.

**Analogue Complexes.** All synthetic steps were performed under a dry dinitrogen atmosphere. The solvents were freshly distilled and degassed. Freshly prepared and sublimed *o*-xylyl-$\alpha,\alpha'$-dithiol was employed.

**Tetraethylammonium Bis(*o*-xylylenedithiolato)ferrate(III).** The synthetic analogue of the rubredoxin Fe–S site, $Fe(S_2\text{-}o\text{-}xyl)_2^-$, was prepared as described in ref 20 except that lithium ethoxide was substituted for sodium ethoxide. Since LiCl is soluble in ethanol only one filtration step was required to isolate the product.

**Tetraethylammonium Bis(*o*-xylylenedithiolato-$d_8$)ferrate(III).** The analogue with deuterium substituted for the eight methylene H atoms was prepared by the preceding procedure, utilizing the ligand *o*-xylylene-$d_4$-$\alpha,\alpha'$-dithiol. The absorption spectrum of the deuterated analogue was identical with the spectrum obtained with the natural abundance analogue.

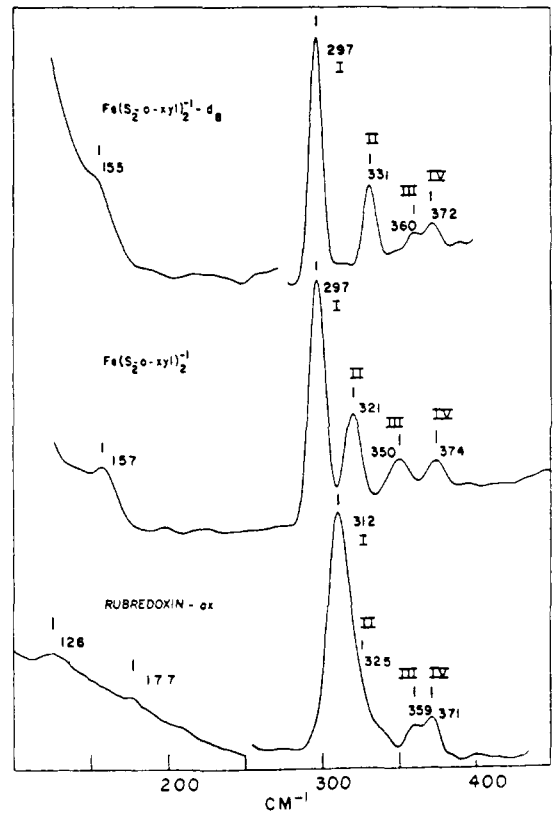


**Figure 1.** Raman spectra of rubredoxin and its *o*-xylylenedithiolate analogue. (Bottom) *D. gigas* $Rd_{ox}$ (1 mM in 0.1 M Tris-HCl buffer, pH 7.4) obtained with a flowing capillary cell by using 4965-Å $Ar^+$ laser excitation (200 mW) and 4-$cm^{-1}$ slit width. (Middle and top) $(Et_4N)$-$Fe^{III}(S_2\text{-}o\text{-}xyl)_2^-$ with H or D at the methylene positions, (~4mM in pyridine), obtained via backscattering from sealed spinning NMR tubes, cooled with cold $N_2$ gas, by using 4825-Å $Ar^+$ laser excitation (50 mW) and 6-$cm^{-1}$ slit width. Bands assigned to Fe–S stretching are labeled I–IV.

***o*-Xylylene-$d_4$-$\alpha,\alpha'$-dithiol, $C_6H_4(CD_2SH)$.** Phthalyl alcohol with the two methylene groups deuterated, $C_6H_4(CD_2OH)_2$, was prepared by a modification of a procedure described in ref 20. A total of 10.2 g of dimethyl phthalate (45 mmol) was added to an ether solution (250 mL) of $LiAlD_4$ (2.4 g, 75 mmol) at a rate sufficient to sustain gentle reflux. When the reaction was complete, water was added dropwise to decompose excess $LiAlD_4$, and the mixture was poured into 100 mL of ice water and then acidified with 10% $H_2SO_4$. The mixture was extracted with ether for 48 h in an ether extractor. Upon evaporation of the ether, an oil remained, which, on being washed with petroleum ether, formed colorless crystals in 75% yield: NMR $\delta$ 7.3 (m, aromatic), 3.5 (s, –O–H). The deuterated $\alpha,\alpha'$-dibromo derivative was prepared by dissolving 6.0 g of $C_6H_4(CD_2OH)_2$ in 12 mL of 49% HBr and 2.9 mL of concentrated $H_2SO_4$, adding 2.5 mL of concentrated $H_2SO_4$ dropwise, then refluxing for $^1/_2$ h. The white crystals were extracted with ether, and washed with water, cold concentrated $H_2SO_4$, and finally $Na_2CO_3$ solution. The ether solution was dried over $CaCl_2$ and evaporated to yield $C_6H_4(CD_2Br)_2$ in 67% yield: NMR $\delta$ 7.35 (m, aromatic). The compound was purified by subliming it twice. $C_6H_4(CD_2SH)_2$ was prepared from $C_6H_4(CD_2Br)_2$ according to the procedure in ref 19: NMR $\delta$ 7.29 (m, aromatic), 1.84 (s).

**$(Et_4N)[Fe(S\text{-}C_6H_4\text{-}p\text{-}CF_3)_4]$.** *p*-(Trifluoromethyl)benzenethiol was added to a solution of $(Et_4N)[Fe(S_2\text{-}o\text{-}xyl)_2]$ in pyridine. A rapid color change occurred due to the displacement of the bidentate ligand by the more acidic monodentate ligand. When the solution was allowed to stand, the color was completely bleached in less than 10 min. This autoreduction process could be prevented by freezing the solution at liquid $N_2$ temperature, immediately following the addition of HS-$C_6H_4$-*p*-$CF_3$. The frozen solution was stable for several hours.

***p*-(Trifluoromethyl)benzenethiol.** A solution of *p*-(trifluoromethyl)-bromobenzene (11.25 g, 50 mmol) in ether (50 mL was added dropwise, with stirring, to 1.215 g (50 mmol) of Mg, under argon, with gentle

(4) (a) Long, T. V.; Loehr, T. M. *J. Am. Chem. Soc.* **1970**, *92*, 6384. (b) Long, T. V.; Loehr, T. M.; Allkins, J. R.; Lovenberg, W. *J. Am. Chem.* **1971**, *93*, 1809.

(5) (a) Yamamoto, T.; Rimal, L.; Heyde, M. E.; Palmer, G., unpublished results, 1972, cited in ref 5b. (b) Eaton, W. A.; Lovenberg, W. In "Iron-sulfur Proteins"; Lovenberg, W., Ed.; Academic Press: New York, 1973; Vol. 2, Chapter 3.

(6) Tang, S.-P. W.; Spiro, T. G.; Mukai, K.; Kimura, T. *Biochem. Biophys. Res. Commun.* **1973**, *53*, 869.

(7) Tang, S.-P. W.; Spiro, T. G.; Antanaitis, B.; Moss, T. H.; Holm, R. H.; Herskovitz, T.; Mortenson, L. E. *Biochem. Biophys. Res. Commun.* **1975**, *62*, 1.

(8) Blum, H.; Adar, F.; Salerno, J. C.; Leigh, J. S., Jr. *Biochem. Biophys. Res. Commun.* **1977**, *77*, 650.

(9) Adar, F.; Blum, H.; Leigh, J. S., Jr.; Ohnishi, T.; Salerno, J. C.; Kimura, T. *FEBS Lett.* **1977**, *84*, 214.

(10) Johnson, M. K.; Hare, J. W.; Spiro, T. G.; Moura, J. J. G.; Xavier, A. V.; Le Gall, J. *J. Biol. Chem.* **1981**, *256*, 9806.

(11) Johnson, M. K.; Spiro, T. G.; Mortenson, L. E. *J. Biol. Chem.* **1982**, *257*, 2447.

(12) Spiro, T. G.; Hare, J.; Yachandra, V.; Gewirth, A.; Johnson, M. K.; Remsen, E. In "Iron-sulfur Proteins"; Spiro, T. G., Ed.; Wiley-Interscience: New York, 1982; Chapter 11.

(13) Yachandra, V.; Hare, J.; Gewirth, A.; Czernuszewicz, R. S.; Kimura, T.; Holm, R. H.; Spiro, T. G. *J. Am. Chem. Soc.*, following paper in this issue.

(14) Czernuszewicz, R.; Johnson, M. K.; Nelson, H.; Remsen, E.; Hare, J.; Gewirth, A.; Yachandra, V.; Holm, R. H.; Spiro, T. G., manuscript in preparation.

(15) Spiro, T. G.; Stein, P. *Annu. Rev. Phys. Chem.* **1977**, *28*, 501.

(16) Moura, I.; Bruschi, M.; Le Gall, J.; Moura, J. J. G.; Xavier, A. V. *Biochem. Biophys. Res. Commun.* **1976**, *75*, 1037.

(17) Moura, I.; Moura, J. J. G.; Xavier, A. V.; Le Gall, J.; Peck, H. D., Jr., unpublished results.

(18) Engle, P. C.; Massey, V. *Biochem. J.* **1971**, *125*, 879.

(19) Mayerle, J. J.; Denmark, S. E.; De Pamphilis, D. V.; Ibers, J. A.; Holm, R. H. *J. Am. Chem. Soc.* **1975**, *97*, 1032.

(20) Lane, R. W.; Ibers, J. A.; Frankel, R. B.; Holm, R. H. *Proc. Natl. Acad. Sci. U.S.A.* **1975**, *72*, 2868.

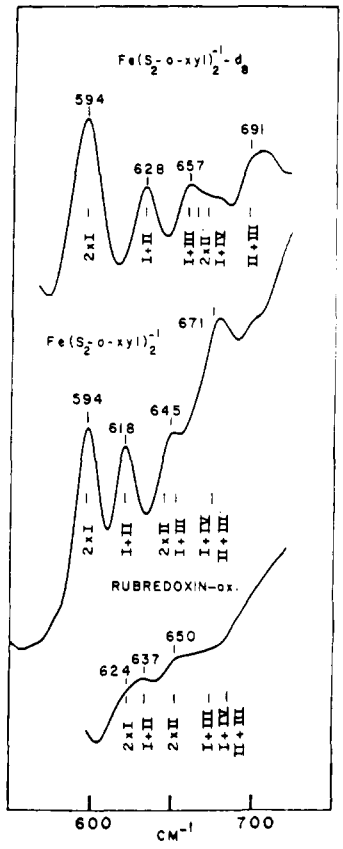


**Figure 2.** Fe–S overtone region Raman spectra of *D. gigas* $Rd_{ox}$ (2.0 mM in 0.1 M Tris-HCl buffer, pH 7.4) and of $(Et_4N)[Fe(S_2\text{-}o\text{-}xyl)_2]$ (~4 mM in acetonitrile). All spectra were obtained via backscattering from sealed spinning NMR tubes cooled with cold $N_2$ gas by using a 4880-Å $Ar^+$ excitation (150 mW) and 10 $cm^{-1}$ slit width. Expected positions of the I–IV overtones and combination levels are marked with horizontal lines.

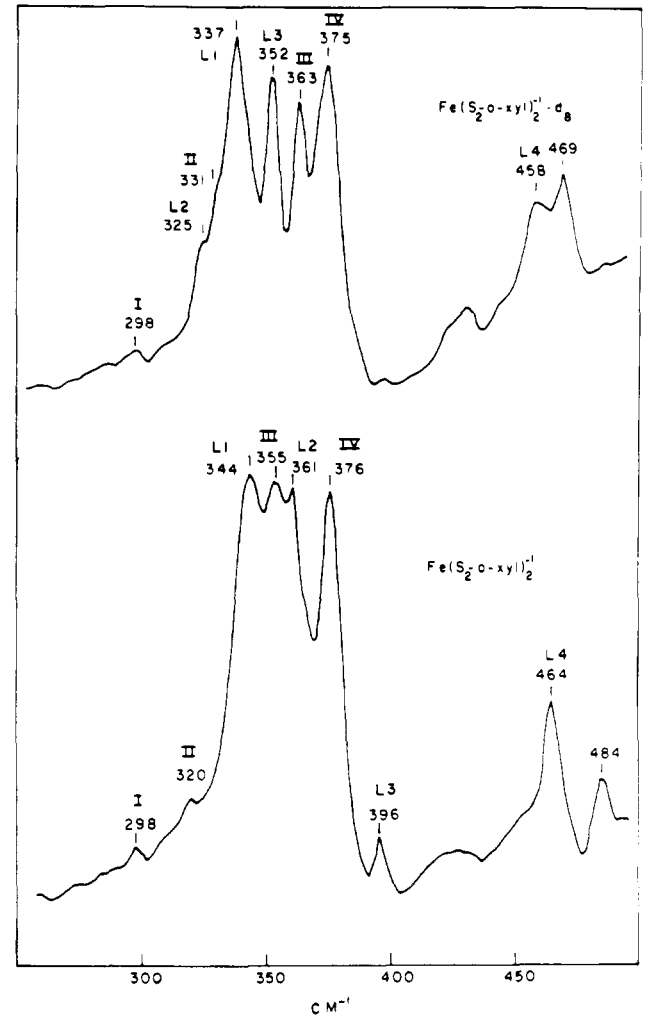


**Figure 3.** Infrared spectra of $Fe(S_2\text{-}o\text{-}xyl)_2^-$ and $Fe(S_2\text{-}o\text{-}xyl)_2^-\text{-}d_8$, obtained with Nujol nulls between polyethylene plates, by using a Digilab FTIR spectrometer, at 4-$cm^{-1}$ resolution. Bands assigned to Fe–S stretching and to ligand modes are labeled I–IV and L1–L4.

heating to maintain the formation of the Grignard compound. The resulting orange-brown solution was refluxed for $^1/_2$ h, and 1.69 g of sulfur (50 mmol) was added slowly, still under argon. HCl (3 N) was added until the aqueous layer was acidic. The separated ether layer was extracted 4 times with 10% NaOH. Acidification of the NaOH extract with 3 N HCl gave a green oil, which was extracted with ether, evaporated, and vacuum distilled to produce a colorless liquid: NMR $\delta$ 7.3 (d of d, $-CH_2-$), 3.5 s, –SH; IR 2570 $cm^{-1}$, $\nu$(S–H).

**Spectra.** In our experience, the best technique for obtaining Fe–S RR spectra is backscattering from a spinning NMR tube[21] containing fairly concentrated (2–4 mM) solutions of the samples. The backscattering geometry minimizes the self-absorption of the scattered light for strongly absorbing materials.[21] The laser beam was directed at the front surface of the upright tube, at an angle of about 45°. The samples were purged with Ar, and the tubes were sealed. A stream of cold $N_2$ was directed at the spinning sample tubes during laser irradiation. Under these conditions the sample damage was negligible, even during prolonged (~5–8 h) spectral acquisition at moderate laser power levels (~50–200 mW), as determined from absorption spectra taken before and after the experiments.

The protein samples were in Tris-HCl buffers, and the analogue complexes were dissolved in pyridine. $Ar^+$ laser excitation (4825, 4880, 4965 Å) near the maximum of the visible absorption band was used to produce maximal enhancement of the Fe–S modes. Spectra were recorded with a Spex 1401 double monochromator equipped with a RCA 31034 photomultiplier and photon counting electronics, under the control of a MINC II (DEC) computer. The data were collected digitally and were smoothed via Gaussian filtration of the Fourier transform of the spectra. The filter function[22] was $e^{A/(t-Bt^2)}$, where the parameters $A$ and $B$ were adjusted empirically to minimize noise without distorting the band shapes. In all cases the band positions were actually determined from the raw data. The criterion for distinguishing weak bands from artifactual fluctuations was the ability to reproduce the feature in separate experiments.

(21) Shriver, D. F.; Dunn, J. B. R. *Appl. Spectrosc.* **1974**, *26*, 319.
(22) Linden, J. C.; Ferrige, A. G. *Prog. Nucl. Magn. Reson. Spectrosc.* **1970**, *14*, 27.

**Table I.** Low-Frequency Vibrational Spectra ($cm^{-1}$) and Methylene Perdeuteration Shifts of *o*-Xylylenedithiol and Its Fe(III) Complex

| | $Fe(S_2\text{-}o\text{-}xyl)_2^-$ | | $Fe(S_2\text{-}o\text{-}xyl)_2^-\text{-}d_8$ | | $(HS)_2$-*o*-xyl, | $(HS)_2$-*o*-xyl-$d_8$, |
|---|---|---|---|---|---|---|
| assignment | R | IR | R | IR | IR | IR |
| Fe–S I | 297 | 298 | 297 | 298 | | |
| Fe–S II | 321 | 320 | 331 | 331 | | |
| $L_1$ | | 344 | | 337 | 319 | 314 |
| Fe–S III | 350 | 355 | 360 | 363 | | |
| $L_2$ | | 361 | | 325 | 334 | 290 |
| Fe–S IV | 374 | 376 | 372 | 375 | | |
| $L_3$ | | 396 | | 352 | 395 | 350 |
| $L_4$ | | 464 | | 458 | 450 | 439 |
| $L_5$ | | 484 | | 469 | | |
| $\delta$(Fe–S) | 157 | | 155 | | | |

## Results

Figure 1 compares low-frequency RR spectra, obtained with excitation in the visible S → Fe charge transfer band, for oxidized *D. gigas* rubredoxin and the synthetic analogue $Fe(S_2\text{-}o\text{-}xyl)_2^-$, with either H or D at the methylene positions. The 500–700-$cm^{-1}$ region, containing the overtones and combinations of the Fe–S fundamentals is shown in Figure 2. Figure 3 shows the infrared spectra of the analogue complexes, while the infrared spectra of *o*-xylylenedithiol itself, in methylene H and D forms, are shown

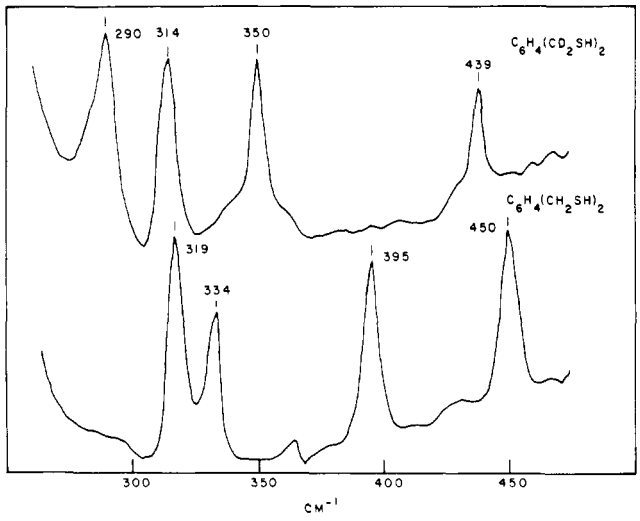


**Figure 4.** Infrared spectra of $C_6H_4(CH_2SH)_2$ and of $C_6H_4(CD_2SH)_2$, obtained with Nujol mulls between polyethylene plates, by using a Digilab FTIR spectrometer at 4-$cm^{-1}$ resolution.

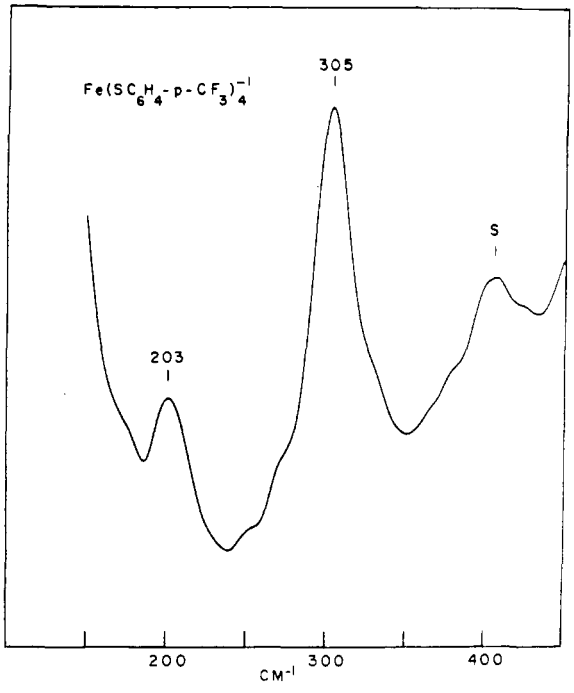


**Figure 5.** Raman spectrum of $(Et_4N)[Fe(S\text{-}C_6H_4\text{-}p\text{-}CF_3)_4]$ in frozen pyridine solution at liquid $N_2$ temperature in a vacuum Dewar by using 4880-Å $Ar^+$ excitation (15 mW) and 10-$cm^{-1}$ slit width. The band marked "S" is a solvent band.

in Figure 4. Table I lists the observed frequencies, in the Fe–S stretching region, for the dithiolates. The RR spectrum of a monodentate analogue, $Fe(S\text{-}C_6H_4\text{-}p\text{-}CF_3)_4^-$, is shown in Figure 5. Figure 6 compares RR spectra for rubredoxins from three species of microorganisms with that of the protein desulforedoxin from *D. gigas*.

## Discussion

**Nontetrahedral Fe–S Vibrational Spectra.** Rubredoxins are small ($M_r \sim 6000$) proteins that contain a single high-spin $Fe^{III}$ ion, which undergoes reversible one-electron reduction at a potential close to −0.05v.[5b] They probably operate in electron transfer reactions, although except for a role in the ω-hydroxylase system in *Pseudomonas oleovorans*,[23] and the characterization of a specific rubredoxin–NAD oxidoreductase in *D. gigas*,[24] their

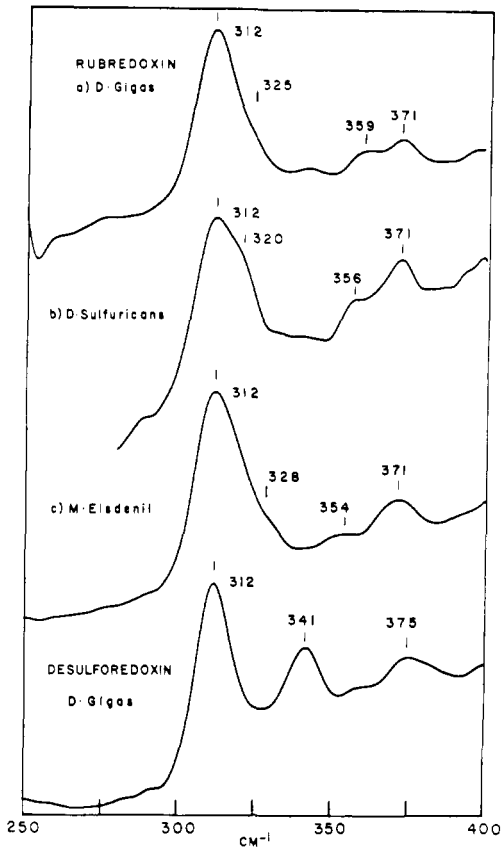


**Figure 6.** Raman spectra of (a–c) oxidized rubredoxin from (a) *D. gigas* (2 mM in 0.2 M Tris-HCl buffer, pH 7.5), (b) *D. sulfuricans* (1 mM in 0.2 M Tris-HCl buffer, pH 7.5), and (c) *M. elsdenii* (1 mM in 0.2 M Tris-HCl buffer, pH 7.5) and (d) desulfuredoxin from *D. gigas* (1 mM in 0.2 M Tris-HCl buffer, pH 7.5). All spectra were obtained via backscattering from a sealed spinning NMR tube cooled with cold $N_2$ gas by using 4880-Å $Ar^+$ excitation (250 mM) and 5-$cm^{-1}$ slit width.

biochemical functions have not been determined. The oxidized proteins are brown, and the visible spectrum is dominated by a broad intense absorption band at ~495 nm, attributable to $-S^- \rightarrow Fe^{III}$ charge-transfer transitions from cysteinate ligands.[5b]

The X-ray crystal structure of oxidized rubredoxin ($Rd_{ox}$) from *Clostridium pasteurianum* has been determined to a resolution of 1.2 Å.[25] The $Fe^{III}$ ion is coordinated by four cysteine side chains, in a tetrahedral arrangement, as shown in Figure 7a. Although one of the Fe–S bonds was initially found to be anomalously short,[26] subsequent refinement has removed the anomaly; all of the Fe–S distances, 2.24–2.33 Å, are within experimental error of the mean value, 2.29 Å. The Fe K edge EXAFS spectrum[27] is superimposable on that of the synthetic analogue complex,[20,27,28] $Fe(S_2\text{-}o\text{-}xyl)_2^-$ ($S_2$-*o*-xyl = *o*-xylylene-α,α′-dithiolate), which has essentially equal Fe–S bonds, of average length 2.267 Å.

The $Rd_{ox}$ RR spectrum, as originally reported by Long and co-workers,[4] was satisfactorily interpreted as arising from a tetrahedral $FeS_4$ complex: a strong, polarized band at 314 $cm^{-1}$, due to the $FeS_4$ breathing mode, $\nu_1(A_1)$; a weak depolarized band at higher frequency, 368 $cm^{-1}$, assigned to the triply degenerate asymmetric Fe–S stretch, $\nu_3(T_2)$; two lower frequency bands, at 150 and 126 $cm^{-1}$, corresponding to the two expected bending modes, $\nu_4(T_2)$ and $\nu_2(E)$. Indeed, the spectrum resembled that of the isoelectronic complex $FeCl_4^-$ (330, 385, 133, and 108 $cm^{-1}$

(23) Lode, E. T.; Coon, M. J. *J. Biol. Chem.* **1971**, *246*, 791.
(24) Le Gall, J.; Dragani, N. *Biochem. Biophys. Res. Commun.* **1966**, *23*, 145.
(25) Watenpaugh, K. D.; Sieker, L. C.; Jensen, L. H. *J. Mol. Biol.* **1979**, *131*, 509.
(26) Watenpaugh, K. D.; Sieker, L. C.; Herriot, J. R.; Jensen, L. H. *Acta Crystallogr.* **1973**, *29B*, 943.
(27) Shulman, R. G.; Eisenberger, P. I.; Teo, B. K.; Kincaid, B. M.; Brown, G. S. *J. Mol. Biol.* **1978**, *124*, 305.
(28) Lane, R. W.; Ibers, J. A.; Frankel, R. B.; Holm, R. H.; Papaefthymiou, G. C. *J. Am. Chem. Soc.* **1977**, *99*, 84.

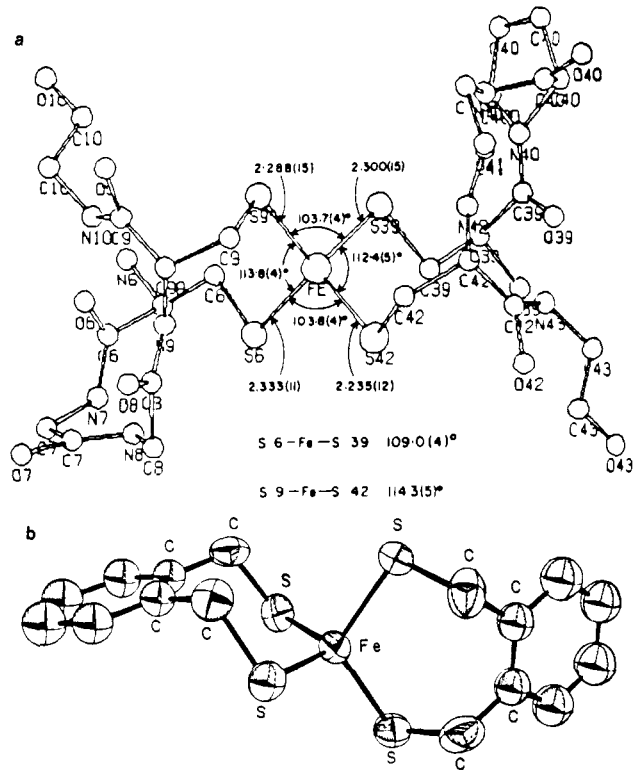


**Figure 7.** (a) A stereo view of the active site of oxidized rubredoxin from *C. pasteurianum*, adapted from ref 25. It illustrates the presence of a $C_2$ axis and the two pairs of Fe–S–C–C dihedral angles, ~90° and ~180°. (b) ORTEP drawing of the molecular structure of $Fe(S_2\text{-}o\text{-}xyl)_2^-$ (from ref 28), viewed down the $C_2$ axis. The dihedral angles about the –S–C bonds are all close to 90°.

for $\nu_1$, $\nu_3$, $\nu_4$, and $\nu_2$[29]) rather closely.

It therefore came as a considerable surprise to us to find that the RR spectrum of $Fe(S_2\text{-}o\text{-}xyl)_2^-$ (Figure 1) is far from being tetrahedral in appearance. It shows four bands in the Fe–S stretching region: two strong ones at 297 and 321 $cm^{-1}$ and two weak ones at 350 and 374 $cm^{-1}$. All of them are polarized, with $\rho \simeq 0.3$. For convenience in the subsequent discussions, we labeled these bands I, II, III, and IV. A single lower frequency band can be resolved, at 155 $cm^{-1}$.

To try and establish whether the four-banded Fe–S region of $Fe(S_2\text{-}o\text{-}xyl)_2^-$ is a peculiarity of the bidentate dithiolate, we attempted to obtain RR spectra of monodentate complexes $Fe(SR)^{4-}$ but found their autoreduction to $Fe^{II}$ species (presumably via disulfide formation) to be much too fast to permit spectral acquisition. Only in the case of $p\text{-}CF_3\text{-}C_6H_4S^-$, whose electron-withdrawing propensity was expected to inhibit oxidation to the disulfide, did we find the $Fe^{III}$ complex to be stable enough (~10 min at room temperature) to freeze a pyridine solution and record its RR spectrum. The result (Figure 5) shows what appears to be a tetrahedral pattern, with a single intense breathing mode at 305 $cm^{-1}$. A bump near 370 $cm^{-1}$, which could be the $T_2$ mode, is unfortunately obscured by a nearby solvent band. Certainly no prominent feature analagous to band II of $Fe(S_2\text{-}o\text{-}xyl)_2^-$ appears on the high-frequency side of the 305-$cm^{-1}$ band.

Reexamination of the $Rd_{ox}$ spectrum (Figure 1), however, shows its apparently tetrahedral pattern[4] to be illusory. The band observed[4] at 368 $cm^{-1}$ is actually two bands, at 371 and 359 $cm^{-1}$. This had been noted by Yamamoto et al.,[5a] who attributed the pair to a splitting of the $T_2$ mode. However, the intense 312-$cm^{-1}$ band, which is broad and asymmetric, also contains two components. This is apparent in the comparison of $Rd_{ox}$ RR spectra from different organisms (Figure 6), which show variable intensities for the high-frequency component of the band. This component can be better resolved in spectra taken with perpendicular polarization, since it is largely depolarized; for $Rd_{ox}$ from *D. gigas* it is located at 325 $cm^{-1}$. We confirm the 126-$cm^{-1}$ band observed by Long et al.[4] but not the 150-$cm^{-1}$ band; rather, we see a weak band at 177 $cm^{-1}$.

(29) Woodward, L. A.; Taylor, M. J. *J. Chem. Soc.* **1960**, 4473.

**Table II.** Calculated Fe–S Stretching Frequency Dependence of $FeS_4$ Symmetry Lowering via $C_2$ Angle Distortions

| $C_2$-related angles, deg[a] | calculated frequencies, $cm^{-1}$ [b] | | | | |
|---|---|---|---|---|---|
| | $T_d$ modes: | $A_1$ | | $T_2$ | |
| | $C_{2v}$ modes: | $A_1$ | $B_1$ | $B_2$ | $A_1$ |
| 109.5, 109.5 | | 312 | 357 | 357 | 357 |
| 105, 105 | | 313 | 351 | 351 | 368 |
| 100, 100 | | 319 | 344 | 344 | 382 |
| 115, 110 | | 313 | 358 | 363 | 350 |
| 115, 105 | | 312 | 352 | 362 | 357 |
| 110, 100 | | 314 | 345 | 357 | 370 |

[a] The cited angles are bisected by an imposed $C_2$ axis. [b] Urey-Bradley force constants taken from ref 35 and 37 and adjusted to the following values: $K_{Fe-S} = 1.26$ mdyn/A; $H_{S-Fe-S} = 0.217$ mdyn/A; $F_{S\cdots S} = (0.144)(3.704/r^9)$ mdyn/A ($r$ is the S···S distance for $FeS_4$ with the specified angles and a Fe–S bond distance of 2.268 Å[27]).

With this additional resolution, the $Rd_{ox}$ RR spectrum in the Fe–S stretching region is seen to be similar to that of $Fe(S_2\text{-}o\text{-}xyl)_2^-$ except that bands II, III and IV are largely depolarized. This similarity is emphasized in the 600–700-$cm^{-1}$ region (Figure 2) where overtone and combination bands involving 2 × I, I + II, 2 × II, I + III, I + IV, and II + III can be identified. For the analogue with deuterated methylene groups the deuteration upshifts of II and III (see discussion below) are reflected in the combination frequencies. The $Rd_{ox}$ spectrum is broad in this region, but the structure corresponds to the expected distribution of overtones and combinations. The involvement of mode II is apparent. We tentatively assign the 700-$cm^{-1}$ band in the RR spectrum of $Fe(S_2\text{-}o\text{-}xyl)_2^-\text{-}d_8$ to C–S stretching. Although the combination level II + III = 691 $cm^{-1}$ is nearby, the band maximizes at a significantly higher frequency.

If it is accepted that the four prominent RR bands, I–IV, all arise primarily from Fe–S stretching, then two fundamental problems must be addressed: (1) The nominally triply degenerate asymmetric stretch is widely split into three components, ranging from 325 to 371 $cm^{-1}$ for $Rd_{ox}$ and 321 to 374 $cm^{-1}$ for $Fe(S_2\text{-}o\text{-}xyl)_2^-$. (2) The most intense RR band, which must arise from the $FeS_4$ breathing mode, is 15 $cm^{-1}$ lower in $Fe(S_2\text{-}o\text{-}xyl)_2^-$ than in $Rd_{ox}$ (297 vs. 312 $cm^{-1}$) despite the fact that the Fe–S distances are the same, within experimental error, in the two structures.

**Angle Distortions.** Since the Fe–S bond lengths are essentially equal, the most obvious source of symmetry lowering lies in the deviations of the S–Fe–S angles from the tetrhedral value, 109.5°. In $Rd_{ox}$ from *C. pasteurianum* these angles range from 114.3° to 103.8°,[25] while for $Fe(S_2\text{-}o\text{-}xyl)_2^-$, the range is 112.6 to 105.8°.[28] To evaluate what effect these relatively small deviations might have on the vibrational spectrum, we carried out normal mode calculations[33,34] on a pseudotetrahedral $FeS_4$ molecule, using a Urey-Bradley force field, to allow for the S···S nonbonded repulsions. Force constants were transferred from ref 35 and 37 and adjusted slightly (see Table II) to produce the following frequencies for tetrahedral $FeS_4$: $\nu_1(A_1) = 312$ $cm^{-1}$; $\nu_3(T_2) = 357$ $cm^{-1}$; $\nu_4(T_2) = 141$ $cm^{-1}$; $\nu_2(E) = 126$ $cm^{-1}$. Next, the tet-

(30) Scott, D. W.; El-Sabban, M. Z. *J. Mol. Spectrosc.* **1969**, *30*, 317.
(31) Ferris, N. S.; Woodruff, W. H.; Tennent, D. L.; McMillin, D. R. *Biochem. Biophys. Res. Commun.* **1979**, *88*, 288.
(32) Larrabee, J. A.; Woolery, G.; Payne, L.; Reinhammar, B.; Spiro, T. G., submitted for publication, 1982.
(33) Wilson, E. B.; Decius, J. C.; Cross, P. C. "Molecular Vibrations"; McGraw-Hill: New York, 1955.
(34) Schachtschneider, J. H. Shell Development Company, Technical Report No. 263-62, 1962.
(35) Geetharani, K.; Sathyanarayanan, D. N. *Spectrochim. Acta, Part A* **1968**, *30A*, 2165.
(36) Nakamoto, K. "Infrared and Raman Spectra of Inorganic and Raman Spectra"; Wiley-Interscience: New York, 1978; p 64.
(37) Sugeta, H. *Spectrochim. Acta, Part A* **1975**, *31A*, 1729.

rahedron was allowed to elongate or flatten or both by varying the angles while keeping a $C_2$ symmetry axis (Table II). The bond lengths were unchanged, and the force constants were also held constant, except that the S···S nonbonded constant was varied in proportion to $r^{-9}$,[36] where $r$ is the S···S separation. Some representative results are given in Table II. The effect on the $A_1$ breathing mode is slight. As might be expected, elongating the tetrahedron splits the $T_2$ mode, raising the $A_1$ component and lowering the two B components, which remain degenerate. Flattening the tetrahedron reverses the splitting. On the scale of the angle variations observed in the crystal structures of Fe-$(S_2$-o-xyl$)_2^-$ and $Rd_{ox}$, the splitting is noticeable (17 $cm^{-1}$ for 105°, 105°, Table II) but it is far from being enough to account for band II, at 321–325 $cm^{-1}$. When the $C_2$-related angles are varied separately, the two B components also split. The situation most closely resembling the range of angles found in the $Rd_{ox}$ structure is the 115°, 105° combination in Table II. Here the three $T_2$ components are spaced at 5 $cm^{-1}$ intervals, from 352 to 362 $cm^{-1}$. We conclude that while angle distortions can produce detectable shifts of the asymmetric Fe–S stretching modes, the widely split spectra that are observed cannot be explained on this basis.

**Fe–S–C–C Conformations.** Another potential perturbation on the Fe–S frequencies is coupling with the S–C–C bending mode of the thiolate ligands. A similar effect has been explored for disulfides,[37] for which appreciable variations in the S–S stretching frequency have been linked to variations in the dihedral angle about the S–C bond, because of the interaction with S–C–C bending. The natural frequency for the latter mode is expected to be ~300 $cm^{-1}$, so that coupling with the Fe–S stretching modes could be substantial. This coupling would be maximal for a Fe–S–C–C dihedral angle of 180°, i.e., a trans conformation of the Fe–S and C–C bonds, since the Fe–S and S–C–C motions would then be in line. A 90° dihedral (staggered conformation) would give minimal coupling, while a 0° angle (cis conformation) would give an intermediate degree of coupling.

In Fe$(S_2$-o-xyl$)_2^-$, the conformation is constrained by the phenyl ring to dihedral angles of ~90° for all four C–S bonds. The complex as a whole has $C_2$ symmetry; Figure 7b shows the structure, viewed nearly along the $C_2$ axis. In $Rd_{ox}$, the conformation is determined by the folding of the polypeptide chain. Figure 7a shows a stereo view of the $FeS_4$ center. There is again an approximate $C_2$ axis, but now the C–S dihedral angle is ~180° for two of the bonds and ~90° for the other two. Thus, the differing dihedral angles provide a basis for differing Fe–S stretching frequencies.

Further normal mode calculations were carried out to evaluate this conformational effect. The model now included ethyl thiolate ligands, with point mass methylene (14) and methyl (15) groups. The S–Fe–S angles were set at 109.5°, as were the S–C–C angles, while the Fe–S–C angles were set at 102.8°, the average value in Fe$(S_2$-o-xyl$)_2^-$. The Fe–S bond lengths were 2.268 Å[27] as before, and standard C–S (1.81 Å) and C–C (1.54 Å) distances were used. The internal coordinate set contained all the bond stretching, angle bending, and torsion displacements. To the Urey-Bradley force constants used previously for the $FeS_4$ calculation were added C–S and C–C stretching,[37] S–C–C[37] and Fe–S–C[35] bending, C–S[37] and Fe–S[35] torsion, and C···S[37] and Fe···C[35] nonbonded force constants. They were adjusted slightly, to the values shown in the Table III footnote, to bring the calculated Fe–S frequencies approximately into line with the RR spectra. Subsequently the force constants were held constant, while the Fe–S–C–C dihedral angles were systematically varied in pairs, keeping a molecular $C_2$ axis. The other dihedral angle, S–Fe–S–C, was held at 180°, close to the value observed in $Rd_{ox}$[25] (Figure 7a). In separate calculations this angle was allowed to vary, but the effect on the Fe–S stretching frequencies was negligible.

Representative results of these calculations are summarized in Table III; some interesting trends are revealed. As expected, the $\nu$(Fe–S), $\delta$(S–C–C) coupling is least for $\tau$(Fe–S–C–C) = 90°, intermediate for 0° and greatest for 180°. The effect is largest for the $A_1$ Fe–S breathing mode, which is closest in frequency to the C–C–S bend. This is illustrated in Figure 8, which shows

**Table III.** Calculated[a] Fe–S Stretching Frequencies ($cm^{-1}$) for a $Fe(SCH_2CH_3)_4$ Model, with Various $C_2$-Related Pairs of Fe–S–C–C Dihedral Angles

| Fe–S–C–C dihedral angles, deg | $C_2$ modes | | | |
|---|---|---|---|---|
| | A | B($x$, $y$) | B($x$, $y$) | A($z$) |
| 90, 90 | 293.2 (42)[b] | 345.0 (90) | 345.0 (90) | 350.4 (100) |
| 0, 0 | 325.6 (42) | 354.8 (87) | 354.8 (87) | 364.8 (86) |
| 0, 90 | 308.1 (60) | 354.8 (87) | 345.0 (99) | 359.4 (90) |
| 0, 180 | 330.6 (45) | 354.8 (87) | 366.0 (79) | 368.5 (85) |
| 30, 180 | 327.1 (46) | 351.6 (90) | 366.0 (79) | 367.3 (85) |
| 60, 180 | 317.2 (55) | 345.3 (99) | 366.0 (79) | 365.2 (86) |
| 90, 180 | 312.2 (68) | 344.9 (99) | 366.0 (79) | 364.7 (82) |
| 120, 180 | 324.5 (52) | 353.4 (88) | 366.0 (79) | 366.4 (86) |
| 150, 180 | 323.7 (47) | 362.4 (81) | 366.0 (79) | 369.6 (86) |
| 180, 180 | 336.5 (48) | 366.0 (79) | 366.0 (79) | 371.3 (84) |

[a] Urey-Bradley force constants taken from ref 35 and 37 and adjusted to the following values: $K_{Fe-S} = 1.17$, $K_{C-S} = 2.5$, $K_{C-C} = 2.5$, $H_{S-Fe-S} = 0.217$, $H_{Fe-S-C} = 0.15$, $H_{S-C-C} = 0.15$, $F_{S\cdots S} = 0.08$, $F_{C\cdots Fe} = 0.05$, $F_{C\cdots S} = 0.43$, $\tau_{-C-S-} = 0.05$, and $\tau_{-Fe-S-} = 0.05$ (mdyn/Å for $K$, $H$, and $F$; mdyn Å for $\tau$). [b] The contribution of Fe–S stretching to the potential energy distribution is in parentheses.

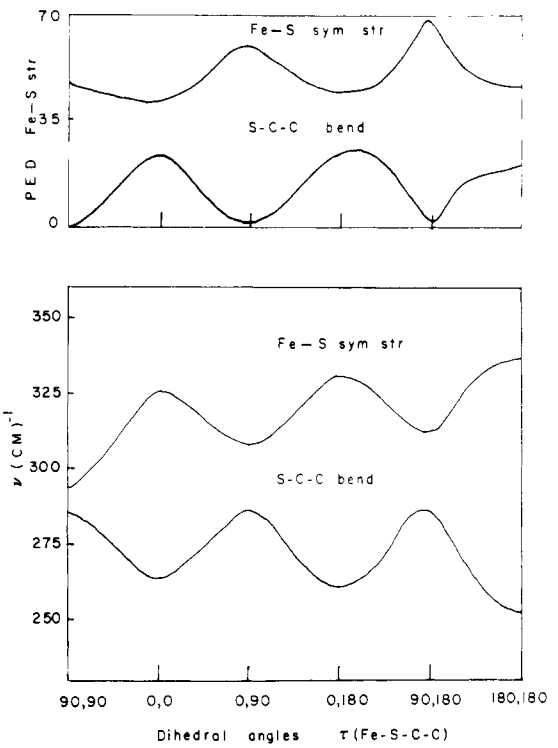


**Figure 8.** Calculated dependence on the Fe–S–C–C dihedral angles ($C_2$ symmetry) of the Fe–S symmetric stretching and the S–C–C bending modes and of the contribution of Fe–S stretching to the potential energy distribution of these modes.

the trends in the two frequencies and the contributions to the potential energy of the $A_1$ Fe–S mode, as the $C_2$-related dihedral angles are varied from 90° through 0° to 180°. When both angles are 90°, C–C–S bending does not contribute to $\nu$(Fe–S), and both frequencies are close to 290 $cm^{-1}$. The coupling is turned on as $\tau$(Fe–S–C–C) decreases or increases and reaches a maximum (20–30% S–C–C contribution to the PED) when both pairs of angles are 0° or 180°; if one of the pairs is 90°, the modes are largely decoupled. There is an underlying trend of increasing $\nu$(Fe–S)($A_1$) from $\tau$ = 90°, 90° (293 $cm^{-1}$) to 0°, 0° (325 $cm^{-1}$) to 180°, 180° (336 $cm^{-1}$). Frequencies for other combinations of angles are close to averages of these limiting frequencies, e.g., at $\tau$ = 90°, 180° $\nu$(Fe–S)($A_1$) = 312 $cm^{-1}$, close to the average (314 $cm^{-1}$) of the 90°, 90° and 180°, 180° values. It is of particular interest that the calculated $A_1$ mode frequencies for 90°, 90° and 90°, 180° are close to the observed frequencies of

band I for $Rd_{ox}$ (312 $cm^{-1}$) and $Fe(S_2$-*o*-xyl$)_2^-$ (297 $cm^{-1}$), which have these conformations. We conclude that the differing conformations are a plausible explanation of the observed frequency difference and, conversely, that the band I frequency is a sensitive monitor of the conformation about the S–C bond in rubredoxins.

Table III shows a similar trend for the highest frequency Fe–S stretch, which is the A component of the tetrahedral $T_2$ mode. However, the effect is smaller, due to the larger frequency difference, and the total range of variation, from 90°, 90° to 180°, 180°, is only 21 $cm^{-1}$, compared to 43 $cm^{-1}$ for the breathing mode. The A component of the $T_2$ mode is split from the two B components even when all the dihedral angles are identical, because it can interact with the breathing mode in $C_2$ symmetry, while the B components cannot. The B modes do nevertheless couple somewhat with the S–C–C bend and show parallel frequency upshifts as the dihedral angles are rotated from 90° (345 $cm^{-1}$) through 0° (355 $cm^{-1}$) to 180° (366 $cm^{-1}$). For $\tau$ = 90°, 90°, both B modes are at 345 $cm^{-1}$, only 5 $cm^{-1}$ below the A mode, while for 90°, 180°, one of the B modes is nearly coincident with the A mode (366 and 365 $cm^{-1}$) while the other B mode is 20 $cm^{-1}$ lower (345 $cm^{-1}$). Neither of these patterns corresponds to the observed spectra for $Fe(S_2$-*o*-xyl$)_2^-$ or $Rd_{ox}$. We conclude that while the S–C conformations can influence the Fe–S splitting pattern, this is not the dominant effect in producing the apparently very wide splitting in both $Fe(S_2$-*o*-xyl$)_2^-$ and $Rd_{ox}$.

**Methylene Involvement.** We considered the possibility that band II is not a fundamental at all but rather the result of a Fermi resonance between band I and the overtone of a bending mode. For $Fe(S_2$-*o*-xyl$)_2^-$, the overtone of the band observed at 157 $cm^{-1}$ (Figure 1), which is probably S–Fe–S bending in character, is a plausible candidate for Fermi resonance with band I. Thinking to perturb the bending frequency and thereby alter the proposed Fermi resonance, we deuterated the methylene groups of the $S_2$-*o*-xyl ligand. The result, shown in Figure 1, was surprising. While the 157-$cm^{-1}$ band did shift down by 2 $cm^{-1}$, there was no effect at all on band I; a Fermi resonance with band I is therefore excluded. However, *both* band II and band III shifted *up*, by 10 $cm^{-1}$, while band IV shifted down by 2 $cm^{-1}$.

Deuteration upshifts imply significant alterations in the normal mode compositions, associated with the mass change. They can usually be understood in terms of an energy crossing with an interacting hydrogenic mode at higher frequency. If the latter shifts down upon deuteration to a frequency lower than the mode in question, the interaction is relieved, or even reversed, resulting in an upshift. Evidence for this mechanism can be found in the IR spectra of $Fe(S_2$-*o*-xyl$)_2^-$ (Figure 3) and of *o*-xylylene-$\alpha,\alpha'$-dithiol itself (Figure 4). The latter shows four prominent absorptions between 250 and 500 $cm^{-1}$ (labeled $L_1$ to $L_4$, see Table I), all of which show pronounced downshifts on methylene perdeuteration. From the intensity patterns it appears that the 334- and 395-$cm^{-1}$ bands ($L_2$ and $L_3$) both shift by fully 45 $cm^{-1}$, while the 319- and 450-$cm^{-1}$ bands ($L_1$ and $L_4$) shift by 5 and 11 $cm^{-1}$.

In the IR spectrum of $Fe(S_2$-*o*-xyl$)_2^-$, we can locate the Fe–S modes I, II, III, and IV at 298, 320, 355, and 376 $cm^{-1}$ and at 298, 331, 363, and 375 $cm^{-1}$ for $Fe(S_2$-*o*-xyl$)_2^-$-$d_8$, essentially the same frequencies as observed in the RR spectra. The remaining bands can be correlated with $L_1$–$L_4$ of the dithiol (see Table I), and an additional band ($L_5$) appears at 484 $cm^{-1}$. $L_1$, $L_2$, and $L_4$ are at appreciably higher frequencies in the $S_2$-*o*-xyl complex (319 → 344, 334 → 361, and 450 → 464 $cm^{-1}$). These differences may be due to a ligand conformation change, as well as the effects of replacing the S–H protons with $Fe^{III}$. The methylene deuteration frequency shifts, however, are of similar magnitude in the complex as in the dithiol. As a result of these shifts $L_2$ crosses over Fe–S band II, while $L_3$ crosses over band III. Thus, the deuteration upshifts of bands II and III are explicable in terms of the interaction of these Fe–S modes with nearby ligand modes having appreciable hydrogenic character.

What these modes are is not easy to say with any precision. Methylene rocking and twisting modes are generally assigned above 600 $cm^{-1}$, but it is clear from a number of studies that these coordinates mix appreciably into lower frequency skeletal modes.[38,39] It is possible that these modes couple differentially to the in- and out-of-phase combinations of Fe–S stretches in a given chelate ring, thereby producing the large splitting among the components of the tetrahedral $T_2$ mode.

**Rubredoxins and Desulforedoxins.** Figure 6 compares RR spectra for $Rd_{ox}$ from three different organisms. The spectral patterns are very similar. Likewise, the reported RR spectrum of $Rd_{ox}$ from *C. pasteurianum*[4] was similar, although the resolution was insufficient to distinguish bands II and III. The fact that the band I position, 312 $cm^{-1}$, is identical for all of these proteins indicates that the cysteine C–S dihedral angles have the same $C_2$-related 90°, 180° pattern as in *C. pasteurianun*,[25] since our calculations show the breathing mode frequency to be sensitive to these angles. This is not surprising, since the primary structure of Rd from *C. pasteurianum*, *D. gigas*, and *M. elsdenii*[41] show the same pattern in the region of the binding site (Figure 7a), namely, pairs of cysteines separated by two other residues.

Subtle variations are nevertheless seen in the positions and relative intensities of bands II and III. These are the same bands that show sensitivity to methylene deuteration in $Fe(S_2$-*o*-xyl$)_2^-$. We infer that the $Rd_{ox}$ conformations do differ slightly, although in the absence of a clearer understanding of the nature of the couplings responsible for the band II and III positions, it is idle to speculate on what these differences are.

The bottom spectrum in Figure 6 is of desulforedoxin from *D. gigas*. This is a rubredoxin-like protein,[16] with absorption,[42] Mössbauer,[43] and EPR[43] spectra that are not quite the same as those of rubredoxin. Its RR spectrum shows the same four-banded pattern (band III is weak and its frequency cannot be determined reliably) as $Rd_{ox}$. The band I frequency, 312 $cm^{-1}$, is the same, suggesting 90°, 180° C–S dihedral angles in desulforedoxin as in $Rd_{ox}$. Band II, however, is appreciably upshifted, to 341 $cm^{-1}$. A possible source of this difference is a change in the S–Fe–S angles, since our calculations show deviations from a tetrahedral $FeS_4$ unit to influence bands II–IV but not band I. This possibility is of interest in connection with the difference in primary structure that has been noted for desulforedoxin.[16] While the known rubredoxin sequences have two pairs of cysteines, each pair having two intervening residues, in desulforedoxin one of the cysteine pairs has no intervening residues. The adjacency of the binding groups might lead to a distortion of the tetrahedral $FeS_4$ angles.[40] It has also been suggested[40] that, since the protein is dimeric, the adjacent cysteine might be bound, with less strain, to separate iron atoms, if the latter are held between the subunits.

**Acknowledgment.** We thank Prof. Jean LeGall and the University of Georgia Fermentation Plant for generously providing the bacteria from which the proteins used in this study were isolated and Prof. Antonio Xavier and Dr. Jose Moura for helpful discussions. This work was supported by National Institutes of Health Grant GM 113498 (to T.G.S.)

**Registry No.** $Fe(S_2$-*o*-xyl$)_2^-$, 57456-64-1; $Fe(SCH_2CH_3)_4$, 86689-78-3; $(Et_4N)[Fe(S_2$-*o*-xyl$)_2^-$-$d_8$], 86847-02-1; dimethyl phthalate, 131-11-3; $C_6H_4(CD_2OH)_2$, 86847-05-4; $C_6H_4(CD_2Br)_2$, 86847-06-5; $C_6H_4(CD_2SH)_2$, 86847-07-6; $(Et_4N)[Fe(S$-$C_6H_4$-*p*-$CF_3)_4]$, 86847-04-3; *p*-(trifluoromethyl)benzenethiol, 825-83-2; *p*-(trifluoromethyl)bromobenzene, 402-43-7; $Fe(S_2$-*o*-xyl$)_2^-$-$d_8$, 86847-01-0; $(HS)_2$-*o*-xyl, 41383-84-0.

(38) Miller, F. A.; Golob, H. R. *Spectrochim. Acta* **1964**, *20*, 1517.
(39) Weiser, H.; Laidlaw, W. G.; Krueger, P. J.; Fuhrer, H. *Spectrochim. Acta, Part A* **1968**, *21A*, 1055.
(40) Xavier, A. V.; Moura, J. J. G.; Moura, I. *Struct. Bonding (Berlin)* **1981**, *43*, 187.
(41) Bachmayer, H.; Yasanodu, K. T.; Peel, J. L.; Mayhew, S. *J. Biol. Chem.* **1968**, *243*, 1022.
(42) Moura, I.; Moura, J. J. C.; Santose, M. H.; Xavier, A. V.; Le Gall, J. *FEBS Lett.* **1979**, *107*, 419.
(43) Moura, I.; Huynh, B. H.; Hausinger, R. P.; Le Gall, J.; Xavier, A. V.; Munck, E. *J. Biol. Chem.* **1980**, *255*, 2493.

# Resonance Raman Spectra of Spinach Ferredoxin and Adrenodoxin and of Analogue Complexes

**Vittal K. Yachandra,[†] Jeffrey Hare,[†] Andrew Gewirth,[†] Roman S. Czernuszewicz,[†] T. Kimura,[‡] Richard H. Holm,[§] and Thomas G. Spiro*[‡]**

*Contribution from the Departments of Chemistry, Princeton University, Princeton, New Jersey 08544, Wayne State University, Detroit, Michigan 48202, and Harvard University, Cambridge, Massachusetts 02138.* *Received September 7, 1982*

**Abstract:** Resonance Raman spectra of oxidized spinach ferredoxin and adrenodoxin show six and seven bands in the Fe-S stretching region (280-430 $cm^{-1}$). Reconstitution of the proteins with labile $^{34}S$ using rhodanese and $^{34}SSO_3^{2-}$ produced isotope shifts allowing identification of all four $Fe_2S_2$ bridging modes and two (three for adrenodoxin) of the four expected Fe-S(Cys) terminal modes. Similar spectra are observed for the analogue complexes $Fe_2S_2(S_2\text{-}o\text{-xyl})_2^{2-}$ ($S_2$-*o*-xyl = *o*-xylylenedithiolate) and $Fe_2S_2Cl_4^{2-}$, but they show the expected $D_{2h}$ selection rules, and IR-active modes are absent or weak in the Raman spectra. All eight (bridging plus terminal) stretching modes were located via IR as well as Raman spectroscopy and were calculated with reasonable accuracy by using a Urey-Bradley force field scaled to the crystallographically determined interatomic distances. The spinach ferredoxin and $Fe_2S_2(S_2\text{-}o\text{-xyl})_2^{2-}$ frequencies are very similar, but adrenodoxin shows appreciably different terminal frequencies, suggestive of conformational differences of the ligated cysteines. The strong activation of IR modes in the protein Raman spectra implies a protein-induced inequivalence of the two ends of the $Fe_2S_2$ complex, which may contribute to the known localization of the added electron in the reduced form. This influence is suggested to be due to enhanced H bonding to the cysteine sulfur atoms at one end of the complex, consistent with available crystal structure data. Reduction of adrenodoxin shifts the bridging frequencies 16-24 $cm^{-1}$ to lower frequency, consistent with the expected weakening of the bridging bonds. The terminal modes, however, were unobserved, plausibly due to a loss of enhancement associated with weakened terminal S → Fe charge transfer intensity, except for a weak band at 308 $cm^{-1}$. At higher frequencies, 550-850 $cm^{-1}$, the protein spectra showed weak bands associated with the Fe-S overtone and combination levels. Previously reported spin-ladder Raman bands of adrenodoxin and spinach ferredoxin were not observed and are attributed to artifacts produced by laser-induced protein damage. A very broad (~200 $cm^{-1}$) and weak feature at ~1000 $cm^{-1}$ in the adrenodoxin spectrum might possibly be due to the $S = 0 \rightarrow 1$ electronic transition of the spin-coupled $Fe^{3+}$ ions.

Proteins containing two Fe atoms and two labile S atoms function as one-electron redox components in a wide range of biological electron transfer chains.[1,2] The first to be isolated were ferredoxins from chloroplasts, which are electron carriers on the reducing side of the photosynthetic chain.[3] Another class of 2-Fe proteins is involved in providing electrons to monooxygenase (cytochrome P-450) enzymes, e.g., in the steroid hydroxylation complex of mammalian adrenal gland mitochondria (adrenodoxin)[4] or the camphor hydroxylation complex of the bacterium *Pseudomonas putida* (putidaredoxin).[5] The representatives of these two classes of 2-Fe proteins, while similar in many respects, show differences with respect to their redox potentials,[4,6a] magnetic susceptibility,[6b] EPR,[6c] and MCD[6d] spectra.

The unusual EPR spectrum generated upon reduction drew initial attention to these proteins[7] and led Gibson and co-workers[8] to propose a model involving spin-coupled $Fe^{2+}$ and $Fe^{3+}$ ions, bridged by sulfide ions, with terminal ligands provided by cysteine side chains.[8] The essential features of this model were confirmed and elaborated by extensive spectroscopic characterization,[9] and its validity was firmly established by the synthetic work of Holm and co-workers,[10-13] who succeeded in synthesizing analogues, using the chelating ligand *o*-xylyl dithiolate to prevent further oligomerization of $Fe_2S_2$ centers. The analogues had essentially the same spectroscopic signatures as the proteins. X-ray crystallography[10,11] showed these complexes to have the expected structure, with tetrahedrally coordinated Fe atoms bridged by S atoms, and gave details of the bond lengths and angles. Only recently has a 2-Fe protein crystal structure begun to emerge.[14] At 2.5 Å the active site shows the Fe atoms bridged by S atoms and coordinated by two cysteine ligands each, as expected.[15]

In this study, we report detailed resonance Raman (RR) spectra of a representative of each of the two main 2-Fe protein classes, ferredoxin from spinach (sp fd) and adrenodoxin (ado). Over the years there have been preliminary reports of RR spectra for these species[16-19] but sufficiently high quality spectra to permit a proper analysis have awaited the development of appropriate experimental techniques, as discussed in the preceding paper.[20] We are now

[†] Princeton University.
[‡] Wayne State University.
[§] Harvard University.

(1) Orme-Johnson, W. H. *Annu. Rev. Biochem.* **1973**, *43*, 159.
(2) Hall, D. O.; Cammack, R.; Rao, K. K. In "Iron in Biochemistry and Medicine"; Jacob, A.; Worwood, M., Eds.; Academic Press: New York, 1974; Chapter 8.
(3) Yocum, C. F.; Siedov, J. N.; Pietro, A. S. In "Iron-Sulfur Proteins"; Lovenberg, W., Ed.; Academic Press: New York, 1973; Vol. I, Chapter 4, p 112.
(4) Estabrook, R. W.; Simpson, K.; Mason, J. I.; Baron, J.; Taylor, W. E.; Simpson, E. R.; Purvis, J.; McCarthy, J. In "Iron-Sulfur Proteins"; Lovenberg, W., Ed.; Academic Press: New York, 1973; Vol. I, Chapter 8, p 193.
(5) Gunsalus, I. C.; Lipscomb, J. D. In "Iron-Sulfur Proteins"; Lovenberg, W., Ed.; Academic Press: New York, 1973; Vol. I, Chapter 6, p 151.
(6) (a) Palmer, G.; Dunham, W. R.; Fee, J. A.; Sands, R. H.; Iizuka, T.; Yonetani, T. *Biochim. Biophys. Acta* **1971**, *245*, 201. (b) Kimura, T.; Tasaki, A.; Watari, H. *J. Biol. Chem.* **1970**, *245*, 4450. (c) Orme-Johnson, W. H.; Sands, R. H. In "Iron-Sulfur Proteins"; Lovenberg, W., Ed.; Academic Press: New York, 1973; Vol. II, Chapter 5, p 195. (d) Thompson, A. J.; Cammack, R.; Hall, D. O.; Rao, K. K.; Briat, B.; Rivoal, J. C.; Badoz, J. *Biochim. Biophys. Acta* **1977**, *493*, 132.
(7) Palmer, G. In "Iron-Sulfur Proteins"; Lovenberg, W., Ed.; Academic Press: New York, 1973; Vol. II, Chapter 8, p 286.
(8) Gibson, J. R.; Hall, D. O.; Thornly, J. M. H.; Whatley, F. R. *Proc. Natl. Acad. Sci. U.S.A.* **1966**, *56*, 987.
(9) Sands, R. H.; Dunham, W. R. *Q. Rev. Biophys.* **1975**, *7*, 443.
(10) Mayerle, J. J.; Denmark, S. E.; DePamphilis, B. V.; Ibers, J. A.; Holm, R. H. *J. Am. Chem. Soc.* **1975**, *97*, 1032.
(11) Mayerle, J. J.; Frankel, R. B.; Holm, R. H.; Ibers, J. A.; Phillips, W. D.; Weiher, J. F. *Proc. Natl. Acad. Sci. U.S.A.* **1973**, *70*, 2429.
(12) Gillum, W. O.; Frankel, R. B.; Fonier, S.; Holm, R. H. *Inorg. Chem.* **1976**, *15*, 1095.
(13) Reynolds, J. G.; Holm, R. H. *Inorg. Chem.* **1980**, *19*, 3257.
(14) Tsukihara, T.; Fukuyama, K.; Tahara, H.; Katsube, Y.; Matsuura, Y.; Tanaka, N.; Kakudo, M.; Wada, K.; Matsubara, H. *J. Biochem. (Tokyo)* **1978**, *84*, 1645.
(15) Fukuyama, K.; Hase, T.; Matsumoto, S.; Tsukihara, T.; Katsube, Y.; Tanaka, N.; Kakudo, M.; Wada, K.; Matsubara, H. *Nature (London)* **1980**, *286*, 522.
(16) Tang, S.-P. W.; Spiro, T. G.; Mukai, K.; Kimura, T. *Biochem. Biophys. Res. Commun.* **1973**, *53*, 869.
(17) Yamamoto, T.; Palmer, G.; Ramai, L.; Gill, D.; Salmeen, I. *Fed. Proc., Fed. Am. Soc. Exp. Biol.* **1974**, *33*, 1372.
(18) Adar, F.; Blum, H.; Leigh, J. S., Jr.; Ohnishi, T.; Salerno, J. C.; Kimura, T. *FEBS Lett.* **1977**, *84*, 214.

0002-7863/83/1505-6462$01.50/0 